Tikrit Journal of Engineering Sciences (2025); 32(3): 2117
DOI: http://doi.org/10.25130/tjes.32.3.7

IRAQI Academic Scientific Journals

ISSN: 1813-162X (Print); 2312-7589 (Online)

Tikrit Journal of Engineering Sciences

available online at: http://www.tj-es.com

TJES Tikrit Journal of Engineering Sciences

Theoretical and Experimental Investigation of Forced Convection of Airflow Over Longitudinally Finned Flat Tube Bank Heat Exchanger

Ahmed H. Ahmed *[a,b], **Maki H. Zaidan** [a], **Manar S.M. Al-Jethelah** [a]

a Department of Mechanical Engineering, College of Engineering, Tikrit University, Tikrit, Iraq.
b Northern Technical University, Hawija Technical Institute, Renewable Energy Research Unit, Kirkuk, Iraq.

Keywords:
Flat tube; Forced convection; Laminar; Longitudinal fins; Staggered.

Highlights:

- *Longitudinal finned-flat tube bank heat exchanger was investigated.*
- *The impact of geometrical parameters was studied.*
- *The effect of the longitudinal pitch was insignificant.*
- *Nu improved up to 128% as Re increased.*

ARTICLE INFO

Article history:

Received	03 Apr. 2024
Received in revised form	23 May 2024
Accepted	09 July 2024
Final Proofreading	11 June 2025
Available online	18 Aug. 2025

Citation: Ahmed AH, Zaidan MH, Al-Jethelah MSM. **Theoretical And Experimental Investigation of Forced Convection of Airflow Over Longitudinally Finned Flat Tube Bank Heat Exchanger**. *Tikrit Journal of Engineering Sciences* 2025; **32**(3): 2117.
http://doi.org/10.25130/tjes.32.3.7

*Corresponding author:
Ahmed H. Ahmed
Northern Technical University, Hawija Technical Institute, Renewable Energy Research Unit.

Abstract: Heat exchangers play a crucial role in various industrial applications. The present paper numerically and experimentally investigated the effects of the Reynolds number (Re), dimensionless transverse pitch ($\widehat{S_T}$), dimensionless longitudinal pitch ($\widehat{S_L}$), dimensionless upstream fin length ($\widehat{L_u}$), dimensionless downstream fin length ($\widehat{L_d}$), and dimensionless fin angle ($\hat{\theta}$) on the heat transfer performance of a longitudinally finned flat tube bank heat exchanger (LFFTBHE) with staggered configurations. The constant surface temperature was assumed. The studied parameters ranges were $223 \leq Re \leq 1114$, $3 \leq \widehat{S_T} \leq 5$, $4 \leq \widehat{S_L} \leq 5$, $0.4 \leq \widehat{L_u} \leq 1$, $0.4 \leq \widehat{L_d} \leq 1.0$, and $0.26 \leq \hat{\theta} \leq 0.78$. The results showed that the average Nu increased steadily with Re, i.e., $6.3 \leq Nu \leq 14.6$. Nu reduced up to 18% with increasing $\widehat{S_T}$. Nu slightly improved with increasing $\widehat{S_L}$ up to 2.1%. Nu decreased with increasing $\widehat{L_u}$ up to 12%. $\widehat{L_d}$ showed a contradictory impact on Nu depending on Re. $\hat{\theta}$ increase improved Nu up to 15.5%. Two correlations were proposed based on the numerical and experimental data.

دراسة نظرية وتجريبية للحمل القسري لتدفق الهواء فوق مبادل حراري ذو أنبوب مسطح مزعنف طولياً

أحمد حسن أحمد[1،2]، مكي حاج زيدان[2]، منار صالح مهدي[2]

[1] معهد الحويجة التقني/ الجامعة التقنية الشمالية/ كركوك - العراق.

[2] قسم الهندسة الميكانيكية/ كلية الهندسة/ جامعة تكريت/ تكريت – العراق.

الخلاصة

المبادلات الحرارية مهمة في العديد من التطبيقات الصناعية. البحث الحالي يدرس نظريًا وتجريبيًا تأثير عدد رينولدز (Re) الخطوة العرضية اللابعدية ($\widehat{ST}$) والخطوة الطولية اللابعدية ($\widehat{SL}$) وطول الزعنفة الامامية اللابعدية ($\widehat{Lu}$) وطول الزعنفة الخلفية اللابعدية ($\widehat{Ld}$) وزاوية الزعنفة اللابعدية ($\hat{\theta}$) على أداء انتقال الحرارة لمبادل حراري ذو أنبوب مسطح مزعنف طوليًا (LFFTBHE) متداخل. تم افتراض درجة حرارة سطحية ثابتة. كان نطاق العوامل المدروسة $223 \le Re \le 1114$, $0.4 \le \widehat{L_d} \le 1.0$, $0.4 \le \widehat{L_u} \le 1$, $4 \le \widehat{S_L} \le 5$, $3 \le \widehat{S_T} \le 5$, $0.26 \le \hat{\theta} \le 0.78$. بينت النتائج تحسن معدل Nu بانتظام بزيادة Re ($6.3 \le Nu \le 14.6$). انخفض Nu لغاية 18% بزيادة $\widehat{S_T}$. تحسن Nu بصورة طفيفة بزيادة $\widehat{S_L}$ لغاية 2.1%. قل Nu بزيادة $\widehat{L_u}$ لغاية 12%. أظهر $\widehat{L_d}$ تأثير متابين على Nu وفق Re. زيادة $\hat{\theta}$ حسنت Nu لغاية 15.5%. تم اقتراح علاقتين ترابطية بالاعتماد على المعطيات العددية والتجريبية.

الكلمات الدالة: أنبوب مسطح، الحمل القسري، صفائحي، زعانف طولية، متداخلة.

1.INTRODUCTION

Heat exchangers are among the many vital industrial processes idealized in longitudinal finned-flat tube bank heat exchangers (LFFTBHE) [1, 2]. Cross-flow heat exchangers explicitly utilize tube banks, and designers still rely on empirical correlations between pressure drop and heat transfer. Heat exchangers with cross-flow tube bundles are highly effective for various chemical and thermal engineering processes [3-10]. Flat tubes are essential in many technical applications, such as complex heat exchangers and car radiators, even though they are not evaluated according to the same standards. Recent advancements in automotive aluminum fabrication technology have made flat-tube heat exchangers more economically viable [11-17]. Heat exchangers with flat tubes are expected to have higher airside heat transfer coefficients and airside pressure reductions than heat exchangers with circular tubes. The pressure loss in flat tubes is expected to be lower than in circular tubes due to the smaller discharge area [18-24]. Flat tube heat exchangers produce less noise and vibration than circular tube heat exchangers [18, 25, 26]. Several studies have investigated the effects of incompressible, steady-state flows on heat transfer through a network of flat tubes situated between two parallel plates using body-fitted coordinate numerical analysis. The studies revealed that the Nusselt number increased with the Reynolds number (Re) [27-30]. It was found that Re varies in the range of $297 \le Re \le 999$ at slow airflow velocities of 1, 2, and 3 m/s, depending on the hydraulic diameter of the tube. In their study, the authors compared cylinders of the same size arranged in circular and elliptical (flat and oval) shapes. According to Mustafa and Abdul Elqadir [31], an increase in the tube's aspect ratio, i.e., eccentricity, results in a higher pressure drop on the air side (external flow). The opposite was true for the internal tube. It was investigated how a cross-flowing elliptical tube affects the convection heat transfer coefficient. Mustafa and Zahi [32] studied air as the working fluid for a Re range of $20 \le Re \le 500$ and a front air assault angle of $\theta \le 90°$. The maximum heat transfer coefficient was recorded at an attack angle of 0°. Abbas et al. [33] experimentally and numerically studied the thermos fluid properties over a semicircular section of a tube placed in cross-flow at different angles. The studied Re range was $2200 \le Re \le 45000$. The greatest Nu number was found at the arc's surface, which is normal to the flow direction (zero angle of attack). Rizal and Ghani [34] experimentally and computationally studied the airflow turbulence in an elliptic tube bundle. The Reynolds number range examined was $5600 \le Re \le 40000$. Tests were conducted with an air attack angle ranging from 0° to 150°, and the four-axis ratios of the tube were 0.25, 0.33, 0.5, and 1. Thermal performance was found to be lowest at 90° and highest at 0° flow of attack when pumping power was kept constant. Ishak et al. [35] experimental investigated heat transfer and fluid flow in a staggered arrangement of flat tube heat exchangers. Investigations included the effects of tube aspect ratios and air attack angles. Nineteen different configurations of heat exchangers were examined, including four aspect ratios (0.18, 0.39, 0.66, and 1), six attack angles from 0° to 150° (in a step of 30°), and air velocity from 2 m/s to 6 m/s. Their results showed that the thermal performance and pressure reduction were controlled by the aspect ratios and attack angles of the tubes. The thermal-hydraulic performance deteriorates in the angle range of $0° \le \theta \le 90°$ due to an increase in pressure drop. The findings showed that compared to tubes with higher aspect ratios, those with lower aspect ratios were more affected by changes in attack angles in terms of their thermal-flow characteristics. The assessments examined the impact of various intake air angles on the heat exchanger's

thermos fluid performance. Tahseen et al. [36] experimentally investigated a finned oval tube heat exchanger running with an angled incoming airflow. Four separate air intake angles (30°, 45°, 60°, and 90°) were all tested between 1300 ≤ Re < 13000. Faghri and Rao [37] experimentally proposed correlations between the Nu number and the airside resistance coefficient. Within constant space, the cylinders' distance from the transversal diagonal axis varied. The longitudinal and diagonal axes of the tube were constrained while being maintained at a constant value. The design included three Bejan numbers, i.e., $10^{-3} \leq Be \leq 10^{-5}$. For each of the three Bejan numbers, the heat exchange between the cylinders and the refrigerant ended when the transverse diagonal axis of the cylinders increased. The heat exchanger's creator used a single row of diamond-shaped tubes to harness natural convection. For all studied Rayleigh numbers, i.e., 10^3, 10^4, and 10^5, heat transfer increased with thinner tubes, i.e., with a low transversal diagonal axis. Naik et al. [38] studied a series of cross-flowing, heated elliptic cylinders. The minor axes of the elliptical tubes and the distance between them were varied, while their major axis was fixed. Dimensionless pressure was reduced with Bejan numbers. It was noted that as the tubes got smaller, the density rate of heat transfer increased. From the preceding discussion, as far as the authors are aware, forced convection along a longitudinally finned flat tube bank heat exchanger (LFFTBHE) has yet to be investigated, considering the effects of the transverse pitch, longitudinal pitch, upstream fin length, downstream fin length, and the back fin angle. The primary challenge in such applications, particularly in thermal systems, is effectively dispersing heat and minimizing pressure drop. Nu was experimentally and theoretically studied for airflow over an LFFTBHE with staggered configurations. The present study covered 223≤Re≤1114. Nu was set as a function of the Reynolds number, Prandtl number, tube-to-tube spacing, dimensionless fin length, and dimensionless fin angle to develop new correlations.

2.COMPUTATIONAL MODELLING

Most computational fluid dynamics computer algorithms that predict fluid flow and heat transfer over a $2D$ bank of tubes in a cross-flow heat exchanger are based on the solution of continuity, momentum, and energy equations. In the initial arrangement of the longitudinal finned flat tube rows analyzed in this research, the tube is placed in front of the dimensionless upstream fin length, $\widehat{L_u} = \frac{L_u}{D_T}$, $(0.4 \leq \widehat{L_u} \leq 1)$. The dimensionless downstream fin length, $\widehat{L_d} = \frac{L_d}{D_T}$ $(0.4 \leq \widehat{L_d} \leq 0.8)$, was positioned in the back of the tube to construct a row of tubes and fins. The dimensionless transfer pitch, $\widehat{S_T} = \frac{S_T}{D_T}$, was $(3 \leq \widehat{S_T} \leq 5)$. The dimensionless longitudinal pitch length, $\widehat{S_L} = \frac{S_L}{D_T}$, was $(4 \leq \widehat{S_L} \leq 5)$. The dimensionless inclination angle of the fin, $\hat{\theta} = \frac{\theta \times \pi}{180}$, was $(0.26 \leq \hat{\theta} \leq 0.78)$. The staggered configurations of the LFFTBHE are assembled in a two-dimensional domain with a defined width (W) and a fixed size (L). The tubes and the fins are isothermal, i.e., T_s=90°C. The working fluid utilized for cooling is air at a constant temperature, T_{in}=T_∞=25℃. The Reynolds number (Re) is within the range of 223≤Re≤ 1114.

2.1.Governing Equations

The basic equations in $2D$ form that describe the flow and thermal fields are the continuity, momentum, and energy equations [39-41]. In two dimensions, the governing equations are expressed as:

$$\frac{\partial u}{\partial x} + \frac{\partial v}{\partial y} = 0 \quad (1)$$

$$\rho\left(u\frac{\partial u}{\partial x} + v\frac{\partial u}{\partial y}\right) = -\frac{\partial p}{\partial x} + \mu\left(\frac{\partial^2 u}{\partial x^2} + \frac{\partial^2 u}{\partial y^2}\right) \quad (2)$$

$$\rho\left(u\frac{\partial v}{\partial x} + v\frac{\partial v}{\partial y}\right) = -\frac{\partial p}{\partial y} + \mu\left(\frac{\partial^2 v}{\partial x^2} + \frac{\partial^2 v}{\partial y^2}\right) \quad (3)$$

$$\left(u\frac{\partial T}{\partial x} + v\frac{\partial T}{\partial y}\right) = \alpha\left(\frac{\partial^2 T}{\partial x^2} + \frac{\partial^2 T}{\partial y^2}\right) \quad (4)$$

where u and v represent the velocity in the x- and y- directions, respectively, ρ represents density, p represents pressure, μ represents viscosity, T represents temperature, and α represents air thermal diffusivity. The following assumptions were applied. The fluid is Newtonian with constant physical properties, the flow is laminar forced convection, incompressible and laminar, small pressure changes, a steady-state flow field with consistent, negligible viscous dissipation, thermal radiation, and heat dissipation, constant surface temperature, constant flow rate, no buoyancy effect, single-phase flow [42]. The studied heat exchanger consists of two rows of staggered layouts. Figure 1 illustrates the physical representation of the present problem. Heat transfer occurs on a horizontal $x-y$ plane via laminar forced convection between the heated, longitudinally finned flat tube bank surface and the intake airflow.

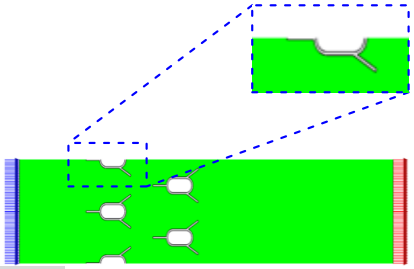

Fig. 1 A Two-Dimension $LFFTBHE$.

The following dimensionless correlations can be used:

$$Pr = \frac{\mu c_p}{k}, Re = \frac{v D_h}{\nu}, Nu = \frac{h D_h}{k}, \widehat{ST} = \frac{ST}{D_T}, \widehat{SL} = \frac{SL}{D_T}, \widehat{Lu} = \frac{Lu}{D_T}, \widehat{Ld} = \frac{Ld}{D_T}, \hat{\theta} = \frac{\theta \times \pi}{180} \quad (5)$$
$$X, Y = \frac{x,y}{Dt}, U, V = \frac{u,v}{(\frac{\Delta p}{\rho})^{\frac{1}{2}}}, \theta = \frac{T - T_o}{T_w - T_o}$$

2.2.Computational Domain and Boundary Conditions

Figure 2 illustrates the physical geometry system of the staggered arrangements of the symmetrical flow in the channels between the *LFFBHE*. Just one channel of flow between finned tubes is required for the computation of the flow and thermal fields. The presented domain shows the side view of the heat exchanger arrangement. The boundary conditions in the physical flow domain are the (A) symmetry plane (V=0), (B) entrance flow (U=1, θ=0), (C) exit flow, and (D) solid surface. The 2D boundary condition and the computational domain for staggered setups of *LFFTHE* are shown in Fig. 2. The following are the applied boundary conditions:

$$A: \quad \frac{\partial U}{\partial Y} = 0, V = 0, \frac{\partial \theta}{\partial Y} = 0 \quad (6)$$

$$B: \quad U = 1, \frac{\partial V}{\partial X} = 0, \theta = 0 \quad (7)$$

$$C: \quad \frac{\partial U}{\partial X} = \frac{\partial V}{\partial X} = 0, \frac{\partial \theta}{\partial X} = 0 \quad (8)$$

$$D: \quad U = V = 0, \theta = 1 \quad (9)$$

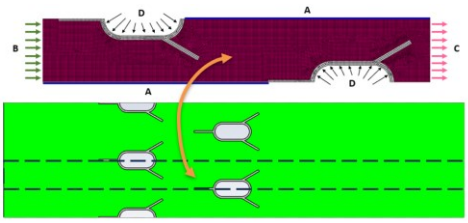

Fig. 2 2D-Computational Domain and Boundary Conditions.

3.EXPERIMENTAL SETUP

A galvanized steel, low-speed, open-circuit wind tunnel, specifically designed and built for forced convection heat transfer purposes, was used for the experimental study. The tests were conducted on a cross-flow heat exchanger located in the wind tunnel to evaluate heat transfer and pressure losses at the laboratories of the Renewable Energy Research Unit, Hawija Technical Institute. The setup consisted of six main sections: an exhaust air section with a variable slide valve to control airflow, an extended region, a reduction unit, a normal unit, a test section, and an AC-powered suction fan. In the test section, a Pitot tube was used to measure the static pressure differential across the rods. An anemometer was used to measure air velocity at any vertical position within the working part. Three power supplies were used. One for managing the speed of the AC motor and two for adjusting the heat source of the cartilage heaters implanted into the flat tube element. To regulate the flow before entering the test portion, metal screens were placed at the entrance of the standard unit. Before the test section, a 400 mm-long normal unit was placed to ensure fully developed flow before arriving at the fin arrangement. Within the wind tunnel, an exhaust fan was installed and directly powered by an electric motor (Model EPMB 4E 250 single phase, 230 V, 0.75 HP, and 50 Hz). Figure 3 shows the schematic representations of the wind tunnel used in this experimental work. Figure 4 shows the velocity profile at the empty case and the wind tunnel calibration of the enlarged region. Figure 5 describes the thermocouple calibration. In the test rig, thirty-two thermocouples were used to measure the temperature, Fig. 6. The thermocouples were distributed as follows: Two at the test rig's layout inlet, eight at tubes surfaces (four on each row), four at the outlet airflow, six on the fin surface (three on each row), eight at radial tube surfaces (four on each row), four at various places on the exterior test section surface to estimate the heat losses, and one to measure the free stream temperature positioned 150 mm from the setup entrance.

4.DATA COLLECTION

The present experimental investigation includes a laminar external airflow. The following air properties relations were adopted within (298 (K) $\leq T_b \leq$ 373(K)) [42]:

$$\rho = [1 \times 10^{-5} T_b^2 - 0.0044 Tb + 1.2868], \frac{kg}{m^3} \quad (10)$$

$$c_P = [-2 \times 10^{-7} T_b^4 + 5 \times 10^{-5} T_b^3 - .0004 T_b^2 + 0.1354 T_b + 1005.4], \frac{J}{(kg\,K)} \quad (11)$$

$$k = [-2 \times 10^{-8} T_b^2 + 8 \times 10^{-5} Tb + 0.0236], \frac{W}{(m\,K)} \quad (12)$$

$$\mu = [-23 \times 10^{-11} T_b^2 + 5 \times 10^{-8} Tb + 2 \times 10^{-5}], \frac{kg}{(m\,s)} \quad (13)$$

$$\alpha = [2 \times 10^{-10} T_b^2 + 1 \times 10^{-7} T_b + 2 \times 10^{-5}], \frac{m^2}{s} \quad (14)$$

$$\nu = [1 \times 10^{-10} T_b^2 + 9 \times 10^{-8} T_b + 1 \times 10^{-5}], \frac{m^2}{s} \quad (15)$$

$$Pr = [5 \times 10^{-7} T_b^2 - 0.0003 T_b + 0.7372] \quad (16)$$

The electrical heat gain rate (q_{in}), the heat carried by air, and heat convected are as follows:

$$q_{in} = E \times I \quad (17)$$

$$q_{air} = \dot{m} \times c_p \times (\overline{T_{out}} - \overline{T_{in}}) \quad (18)$$

$$q_{convection} \cong q_{sup} = \bar{h} A_s [\overline{T_s} - \overline{T_b}] \quad (19)$$

$$\left(\overline{T_b} = \frac{\overline{T_{in}} + \overline{T_{out}}}{2}\right) \quad (20)$$

where V and I represent the applied voltage and current, respectively. $\dot{m}$ is the air mass flow rate, $\overline{T_{out}}$ and $\overline{T_{in}}$ are the temperatures of the air that leaves and enters the system ranging from 20 °C *to* 25 °C, $\overline{T_s}$ is the tube and fins surface temperature, and $\overline{T_b}$ is air bulk temperature. The surface area is a combination of the projected area and the total fins' surface area.

$$A_s = (((((\pi) * 0.01 * 0.13) + (2 * 0.01 * 0.13)) * n) + (((L_u * 0.13 * nu * 3) + (L_d * 0.13 * n_d * 3)) * 2)) \quad (21)$$

where n is the tube number, h_u is the height of upstream fins, n_u is the upstream fins number,

L_u and L_d are the height of upstream and downstream fins, respectively, and n_d is the downstream fins number. The overall heat transfer coefficient was determined from:

$$\bar{h} = \frac{q_{air}}{A_s\left[\overline{T_s} - \left(\frac{\overline{T_{in}} + \overline{T_{out}}}{2}\right)\right]} \quad (22)$$

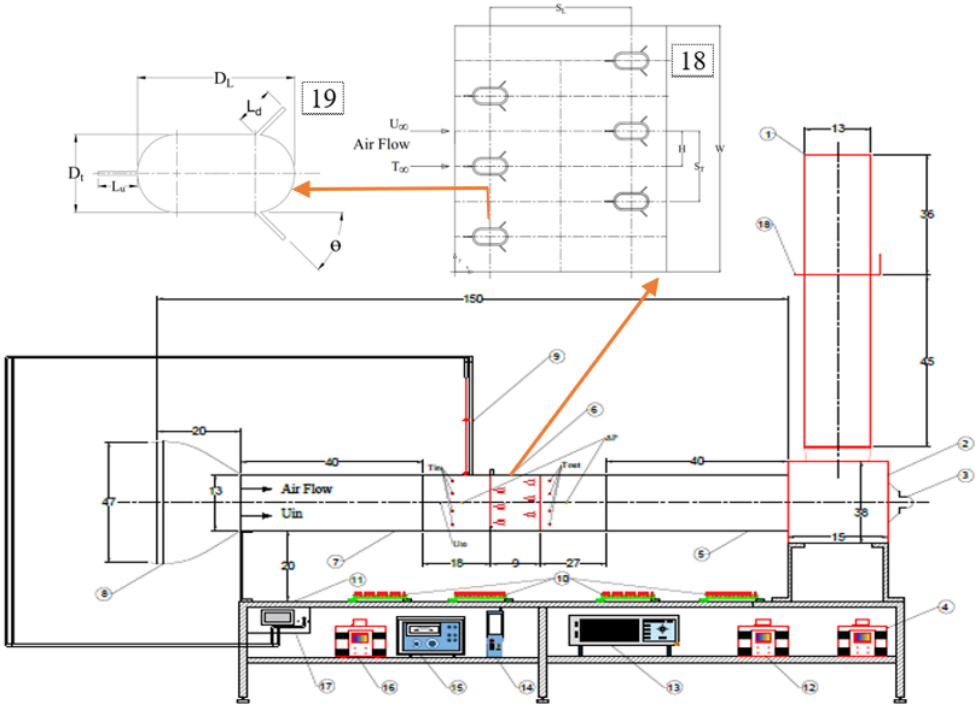

1- Exhaust air section
2- Suction fan
3- A.C motor
4- Controller
5- Extended region
6- Test section
7- Normal unit
8- Reduction unit
9- Pitot tube
10- Pass board
11- Base frame with Stand plate
12- A-C Power supplies the first raw
13- Data logger
14- Hot wire anemometer
15- D-C power supply
16- A-C power supply second raw
17- Pitot tube monitor
18- Rows of LFFTB in cross-flow
19- Front view of longitudinal fin tube

Fig. 3 Schematic Diagram of the Experimental Approach, All Dimensions in mm.

5.EXPERIMENTAL UNCERTAINTY

The experimental investigation adds a wide range of other metrics, including geometrical sizes, heat transfer rates, and fluid flow rates. The errors have been caused in part by these several measuring techniques. The independent and dependent variables interact with one another. Consequently, the influence of individual parameter errors on the ultimate result is considered. When handling experimental uncertainty issues, the guidance was adhered to, and some other influential works on the subject were also reviewed [43-48]. Three categories comprise the sources of error: calibration error, data collection error, and data reduction error. Some mistaken members were bound in any group. Measurement instrument or equipment manufacturers provide a range of information systems, including linearity, precision, drift, slowness, and repeatability. The bias error (B) and precision limit (P) are independent parameters that can be determined by employing a gather root-sum-squares (RSS) technique. Using the root-sum-squares (RSS) approach, the independent parameters, i.e., temperature and dimensions, were identified, including aligned (B) and accuracy errors (P) [49].

$$B = \left[B_1^2 + B_2^2 + B_3^2 + \ldots + B_n^2\right]^{1/2}$$
$$P = \left[P_1^2 + P_2^2 + P_3^2 + \ldots + P_n^2\right]^{1/2} \quad (23)$$

Elemental errors were integrated to obtain 95% for confidence uncertainty (U) using the following relationship:

$$U = [B^2 + P^2]^{1/2} \quad (24)$$

$$B = \pm\left[\left(\frac{1}{2}\text{Resolution}\right)^2 + (\text{Accuracy})^2\right]^{1/2} \quad (25)$$

The average value of the scale is:

$$\bar{\chi} = \frac{1}{n}\sum_{i=1}^{n}\chi_i \quad (26)$$

The standard deviations (σ) are:

$$\sigma_\chi = \left[\frac{1}{n-1}\sum_{i=1}^{n}(\chi_i - \bar{\chi})^2\right]^{1/2} \quad (27)$$

The mean standard deviations ($\sigma_{\bar{\chi}}$) are:

$$\sigma_{\bar{\chi}} = \frac{\sigma_\chi}{\sqrt{N}} \quad (28)$$

It is recommended to use the student-t distribution with a 95% confidence interval and the figure for (N-1) degrees of freedom. One

possible way to express the total accuracy error limitations is as follows:

$$P_\chi = t_{(N-1),95\%} \times \sigma_{\bar{\chi}} \quad (29)$$

It is done to integrate the errors of the elements and produce their 95% confidence interval for the uncertainty. U_χ is found in the following relationship:

$$U_\chi = \pm \left[B^2 + P_\chi{}^2\right]^{1/2} \quad (30)$$

The relative uncertainty is computed as a percentage based on the following:

$$\frac{U_\chi}{\chi}\% = \pm \left(\frac{U_\chi}{\chi}\right) \times 100 \quad (31)$$

The percentage errors for all dependent and independent variables are tabulated in Table 1.

Table 1 Summary of the Experimental Uncertainty.

Parameter	Uncertainty		Parameter	Uncertainty	
	Min. (%)	Max. (%)		Min. (%)	Max. (%)
Dh	0.471726668	0.482661345	Q_{in}	3.575435342	3.968731863
E	1.561026618	1.681105589	Re	3.477968985	3.582075559
h	4.58206256	4.726205438	T_b	0.165648354	0.166320556
I	3.21666501	3.595096188	T_{in}	1.277027153	1.278988323
$\dot{m}$	3.443380188	3.54509105	T_{out}	1.207569404	1.216190702
Nu	4.614230901	4.76218463	T_s	1.029727159	1.033275985
Pr	0	0.405847058	u_{in}	3.427249022	3.522915429
Q_a	3.865992169	3.960127226			

6.RESULTS AND DISCUSSION

Heat transfer for airflow over a *LFFBHE* with staggered configurations is experimentally investigated. The impact of the dimensionless transfer pitch ($3 \le \widehat{S_T} \le 5$), the dimensionless longitudinal pitch length ($4 \le \widehat{S_L} \le 5$), the dimensionless upstream fin length ($0.4 \le \widehat{L_u} \le 1$), the dimensionless downstream fin length ($0.4 \le \widehat{L_d} \le 1.0$), and the dimensionless downstream fin angle ($0.26 \le \hat{\theta} \le 0.78$) on the Nusselt number was studied. The studied Reynolds number range was $223 \le Re \le 1114$. Figure 7 shows the impact of the dimensionless transverse pitch ($\widehat{S_T}$) on the Nusselt number (Nu). The dimensionless transverse pitch range was ($3 \le \widehat{S_T} \le 5$) at $\widehat{S_L}$= 4, $\widehat{L_u}$=$\widehat{L_d}$ =0.8, $\hat{\theta}$= 0.53, and $223 \le Re \le 1214$. Nu was inversely proportional to $\widehat{S_T}$. Increasing the flow cross-sectional area reduced the air velocity. As a result, the thermal boundary layer became thicker, and the heat transfer rate decreased. Therefore, Nu decreased as $\widehat{S_T}$ increased. The highest Nusselt number was 14.3 at $\widehat{S_T}$=3 and Re= 1114. The lowest Nusselt number was 6.2 at $\widehat{S_T}$=5 and Re= 223. The Nu increased with Re. Increasing Re accelerated sweeping the adjacent air layer. Therefore, the thermal layer decreased, resulting in a high heat transfer rate and a high Nusselt number. At $\widehat{ST}$=3, the Nu increased by 104.7% as Re increased from 223 to 1114. At $\widehat{ST}$=5, the Nu increased by 93.2% as Re increased from 223 to 1114. This result is consistent with references [33, 50]. Figure 8 depicts the impact of the dimensionless longitudinal pitch ($\widehat{S_L}$) on the Nusselt number (Nu). The dimensionless longitudinal pitch range was ($4 \le \widehat{S_L} \le 5$) at $\widehat{S_T}$= 3, $\widehat{L_u}$=$\widehat{L_d}$ =0.8, $\hat{\theta}$= 0.53, and $223 \le Re \le 1214$. Changing the dimensionless longitudinal pitch slightly influenced the flow cross-sectional area. As a result, the air velocity insignificantly increased through the configuration. Therefore, increasing $\widehat{S_L}$ insignificantly increased Nu. At Re= 223, the Nu improved by 1.3% as $\widehat{S_L}$ changed from 4 to 5, respectively. At Re= 1114, the Nu improved by 2.1% as $\widehat{S_L}$ changed from 4 to 5, respectively. Figure 9 shows the impact of the dimensionless upstream fin length ($\widehat{L_u}$) on the Nusselt number (Nu). The dimensionless upstream fin length was ($0.4 \le \widehat{L_u} \le 1.0$) at $\widehat{S_T}$= 3, $\widehat{S_L}$= 4, $\widehat{L_d}$ =0.8, $\hat{\theta}$= 0.53, and $223 \le Re \le 1214$. The short upstream fin provided a small contact area with the air, resulting in a lower heat transfer rate between the fin and the air. Therefore, the cold air collided with the hot flat pipe before being significantly heated by the upstream fin. As a result, the thermal boundary layer was thin, resulting in a high heat transfer rate. The long upstream fin provided a larger contact area with the air, thereby preheating it. Therefore, a lower heat transfer rate occurred when the preheated air collided with the hot flat pipe. This result agrees with [51]. At Re= 223, the Nu decreased by 6.5% as $\widehat{L_u}$ changed from 0.4 to 1.0, respectively. At Re= 1114, the Nu decreased by 11.3% as $\widehat{L_u}$ changed from 0.4 to 1.0, respectively.

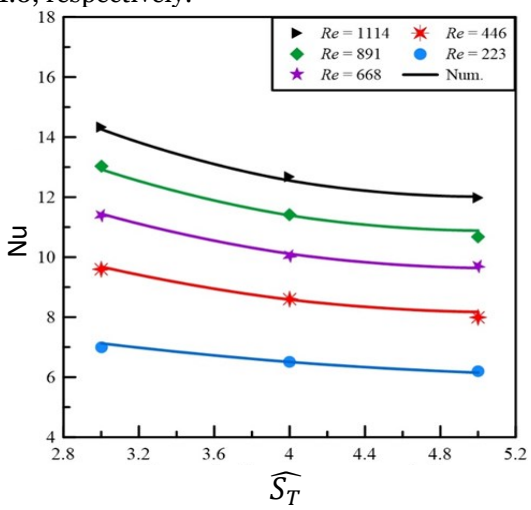

Fig. 7 Impact of $\widehat{S_T}$ on Nu for Various Re ($223 \le Re \le 1214$) at $\widehat{S_L}$= 4, $\widehat{L_u}$=$\widehat{L_d}$ =0.8, and $\hat{\theta}$= 0.53.

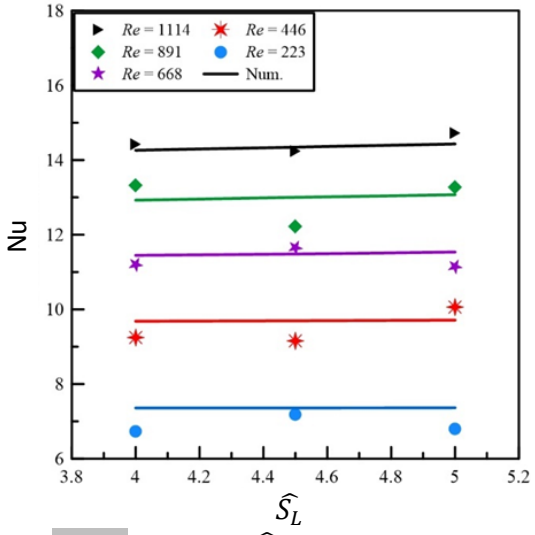

Fig. 8 Impact of $\widehat{S_L}$ on Nu for Various Reynolds Numbers ($223 \leq Re \leq 1214$) at $\widehat{S_T}$= 3, $\widehat{L_u}$=$\widehat{L_d}$ =0.8, and $\hat{\theta}$= 0.53.

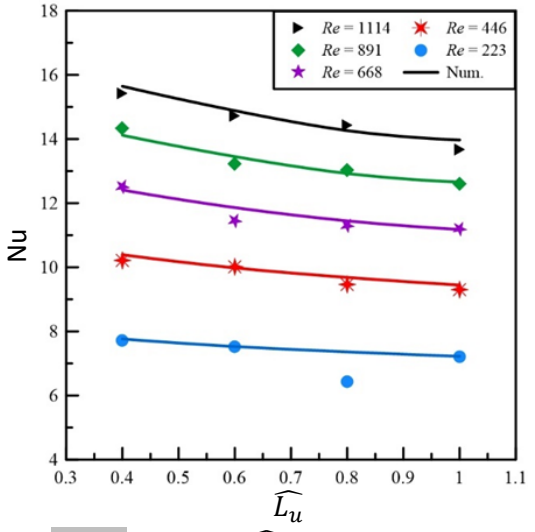

Fig. 9 Impact of $\widehat{L_u}$ on Nu for Various Reynolds Numbers ($223 \leq Re \leq 1214$) at $\widehat{S_T}$= 3, $\widehat{S_L}$= 4, $\widehat{L_d}$ =0.8, and $\hat{\theta}$= 0.53.

Figure 10 shows the impact of the dimensionless downstream fin length ($\widehat{L_d}$) on the Nusselt number (Nu). The dimensionless downstream fin length was ($0.4 \leq \widehat{L_d} \leq 1.0$) at $\widehat{S_T}$= 3, $\widehat{S_L}$= 4, $\widehat{L_u}$=0.8, $\hat{\theta}$= 0.53, and $223 \leq Re \leq 1214$. At low Re, i.e., 223, increasing $\widehat{L_d}$ from 0.4 to 0.8 restricted the airflow. As a result, the thermal boundary layer around the fins increased, and consequently, Nu decreased. Beyond $\widehat{L_d}$= 0.8, the flow cross-sectional area decreased; therefore, the flow velocity increased. Increasing the velocity impact dominated the restriction impact; therefore, Nu increased. For higher Re, i.e., 446-1114, Nu decreased as $\widehat{L_d}$ increased from 0.4 to 0.6 due to restriction impact. Nu increased with $\widehat{L_d}$ beyond 0.6 due to a decrease in flow cross-sectional area, i.e., increasing the flow velocity. The lowest Nu value was 7.6 at Re=223 and $\widehat{L_d}$=0.4. The highest Nu value was 14.9 at Re=1114 and $\widehat{L_d}$=1.0. This result agrees with [52, 53].

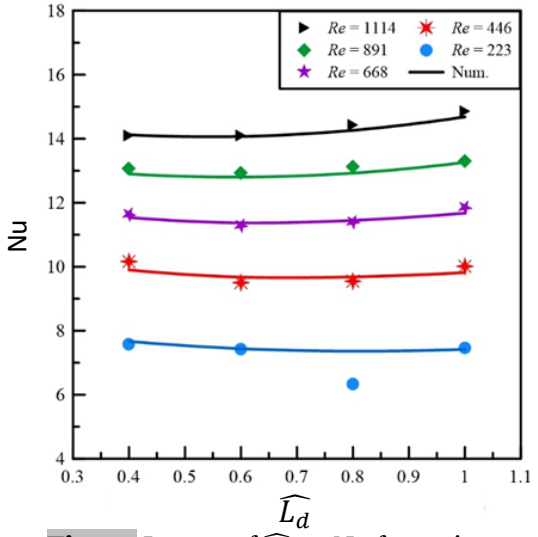

Fig. 10 Impact of $\widehat{L_d}$ on Nu for various Reynolds numbers ($223 \leq Re \leq 1214$) at $\widehat{S_T}$= 3, $\widehat{S_L}$= 4, $\widehat{L_u}$=0.8, and $\hat{\theta}$= 0.53.

Figure 11 shows the impact of the fin angle ($\hat{\theta}$) on the Nusselt number (Nu). The dimensionless downstream fin length was ($0.26 \leq \widehat{L_d} \leq 0.75$) at $\widehat{S_T}$= 3, $\widehat{S_L}$= 4, $\widehat{L_u}$=$\widehat{L_d}$= 0.8, and $223 \leq Re \leq 1214$. Increasing $\hat{\theta}$ increases the flow restriction; as a result, the thermal boundary layer becomes thicker, and Nu decreases. On the other hand, increasing $\hat{\theta}$ increased the flow velocity due to the small flow cross-sectional area. Increasing $\hat{\theta}$ at low Re, i.e., 223, increased the impact of flow restriction, decreasing Nu. However, a further increase in $\hat{\theta}$ increased the flow velocity, thereby increasing Nu. The associated high velocities with high Re and $\hat{\theta}$ values increased Nu. The lowest Nu was 6.8 at Re=223 and $\hat{\theta}$=0.26. The highest Nu was 14.09 at Re=1114 and $\hat{\theta}$=0.79.

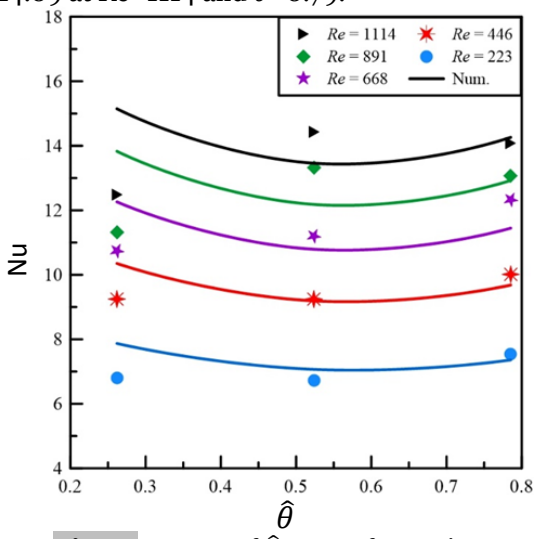

Fig. 11 Impact of $\hat{\theta}$ on Nu for Various Reynolds Numbers ($223 \leq Re \leq 1214$) at $\widehat{S_T}$= 3, $\widehat{S_L}$= 4, and $\widehat{L_u}$=$\widehat{L_d}$= 0.8.

7.NEW DEVELOPED CORRELATIONS

When conducting statistical analysis, the nonlinear regression technique was used. A method for determining the relation between a group of independent parameters or responses and a dependent parameter is called nonlinear regression. To evaluate the models with arbitrary relationships between the independent and dependent parameters, this technique uses iterative processes [54, 55]. The generated models employ the Levenberg-Marquardt approach. Several computer programs, including SPSS, are utilized. The acceptable benchmark for a regression model created to fit test data is the R^2 value. Since all residuals, i.e., the difference between the estimated and actual data values at each test point, are zero, an R^2 value of one denotes a perfect correlation. Equation (32) is used to estimate the mean relative error (MEr) between the empirical and forecasted data and the maximum relative error (Er) for any variable (φ) [56].

$$MEr\ (\%) = \frac{1}{n}\sum_{i=1}^{n} /Er\ (\%)/_i$$

$$\mathbf{Er}\ (\%) = \frac{\left(\varphi_{(expt)} - \varphi_{(pred)}\right)}{\varphi_{(expt)}} \times 100 \qquad \mathbf{(32)}$$

where n denotes the number of experimental data, $\varphi_{(expt)}$ denotes the experimental data, and $\varphi_{(pred)}$ denotes the predicted data.

Based on the present investigation's numerical and experimental results, i.e., which include 85 samples, new correlations for Nu have been proposed. The correlations determine Nu based on Re, Pr, $\widehat{S_T}$, $\widehat{S_L}$, $\widehat{L_u}$, $\widehat{L_d}$, and $\hat{\theta}$. The correlations apply for two staggered rows of $LFFTBHE$ with cross-flows under the conditions below

$$200 \le Re \le 1200, Pr = 0.7185, 0.4 \le \widehat{Lu} \le 1, 0.4 \le \widehat{Ld} \le 1, 3 \le \widehat{ST} \le 5, 4 \le \widehat{SL} \le 5, 0.26 \le \hat{\theta} \le 0.78$$

The general correlation of Nu is given as:

$$Nu = a + \frac{b(\mathrm{RePr})^c}{\left[0.5+\left(\frac{0.8}{\mathrm{RePr}}\right)^d\right]^{-1}} \left(\widehat{Lu}\right)^e \left(\widehat{Ld}\right)^f \left(\widehat{ST}\right)^g \left(\widehat{SL}\right)^i \left(\hat{\theta}\right)^k \qquad \mathbf{(33)}$$

where a, b, ... , and k are correlation constants. Figure 12 displays the predicted values from Eq. (34) alongside the numerical data. The mean deviation was ±5%, and all deviations were within this range. The R^2 score of 99.8% indicates a strong statistical fit.

$$Nu = 1.834 + \frac{1.385(\mathrm{RePr})^{0.503}}{\left[0.5+\left(\frac{0.8}{\mathrm{RePr}}\right)^{20.208}\right]^{-1}} \left(\widehat{Lu}\right)^{-0.130} \left(\widehat{Ld}\right)^{0.019} \left(\widehat{ST}\right)^{-0.454} \left(\widehat{SL}\right)^{0.009} \left(\hat{\theta}\right)^{0.129} \qquad \mathbf{(34)}$$

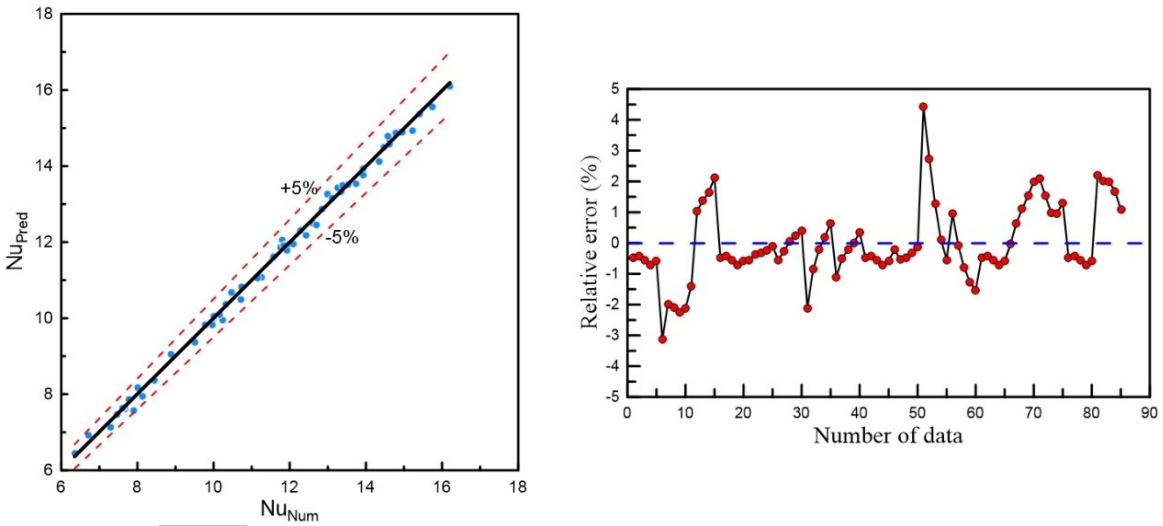

Fig. 12 Correlation and Relative Error of Numerical Nu for $LFFTBHE$.

The predicted values from correlation Eq. (35) and the experimental data are shown in Fig. 13. The deviations were within ±7%, and the relative error was approximately ±13%. The R^2 value was approximately 97.0%, indicating a good statistical fit.

$$Nu = -0.37 + \frac{3.645(\mathrm{RePr})^{0.407}}{\left[0.5+\left(\frac{0.8}{\mathrm{RePr}}\right)^{17.228}\right]^{-1}} \left(\widehat{Lu}\right)^{-0.070} \left(\widehat{Ld}\right)^{-0.012} \left(\widehat{ST}\right)^{-0.381} \left(\widehat{SL}\right)^{-0.125} \left(\hat{\theta}\right)^{0.122} \qquad \mathbf{(35)}$$

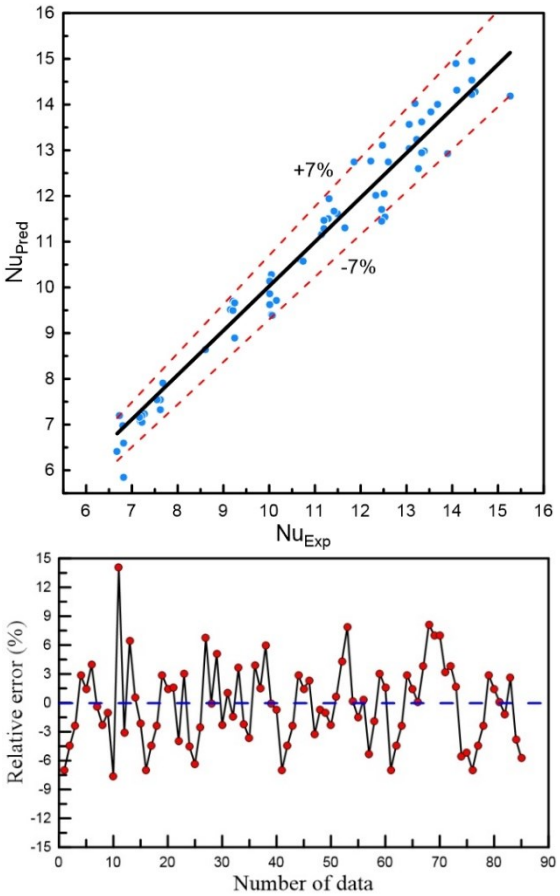

Fig. 13 Correlation and Relative Error of Experimental Nu for *LFFTBHE*.

8.CONCLUSION

The present study numerically and experimentally investigated the thermal performance of a longitudinally finned-flat tube bank heat exchanger. The tube surface temperature was maintained at a constant value. The studied parameters were the dimensionless transfer pitch ($\widehat{S_T}$), the dimensionless longitudinal pitch length ($4 \leq \widehat{S_L} \leq 5$), the dimensionless upstream fin length ($0.4 \leq \widehat{L_u} \leq 1$), the dimensionless downstream fin length ($0.4 \leq \widehat{L_d} \leq 1.0$), and the dimensionless downstream fin angle ($0.26 \leq \hat{\theta} \leq 0.78$) on the Nusselt number was studied. The studied Reynolds number range was $223 \leq Re \leq 1114$. The following conclusions have been attained as a key outcome of the present study.

1- Nu was directly proportional to Re. Nu improved between 83.2%, i.e., at $\hat{\theta}$ =0.26, $\widehat{S_T}$= 3, $\widehat{S_L}$= 4, and $\widehat{L_u}$=$\widehat{L_d}$= 0.8, and 128%, i.e., at $\widehat{L_d}$=0.8, $\widehat{S_T}$= 3, $\widehat{S_L}$= 4, $\widehat{L_u}$=0.8, and $\hat{\theta}$= 0.53, as Re increased from 223 to 1114, respectively.

2- Nu was inversely proportional to the transverse pitch. The highest Nu reduction was 18% as $\widehat{S_T}$ increased from 3 to 5 at Re=891, $\widehat{S_L}$= 4, $\widehat{L_u}$=$\widehat{L_d}$ =0.8, and $\hat{\theta}$= 0.53.

3- The longitudinal pitch insignificantly ($\widehat{S_L}$) improved Nu. The highest improvement was 2.1% at Re=223, $\widehat{S_T}$= 3, $\widehat{L_u}$=$\widehat{L_d}$ =0.8, and $\hat{\theta}$= 0.53 as $\widehat{S_L}$ increased from 4 to 5.

4- Increasing the dimensionless upstream fin length ($\widehat{L_u}$) from 0.4 to 1.0 decreased Nu by 12% at Re=891, $\widehat{S_T}$= 3, $\widehat{S_L}$= 4, $\widehat{L_d}$ =0.8, and $\hat{\theta}$= 0.53.

5- The impact of the dimensionless downstream fin length ($\widehat{L_d}$) on Nu depended on Re. At Re= 223 and 446, increasing $\widehat{L_d}$ from 0.4 to 1.0 reduced Nu by 1.6% and 1.5%, respectively. For Re≥ 668, increasing $\widehat{L_d}$ increased Nu by up to 5.4% at Re=1114.

6- Nu enhanced up to 15.5% as the dimensionless fin angle ($\hat{\theta}$) increased at Re=891, $\widehat{S_T}$= 3, $\widehat{S_L}$= 4, and $\widehat{L_u}$= $\widehat{L_d}$ =0.8.

7- Developed *Nu* correlations showed good agreement with mean deviation for numerical and experimental data, i.e., 5% and 7%, respectively. The anticipated values, which accounted for R^2 99.8% of the numerical and 97.0% of the experimental data, were within relative error of ±5% and ±13%, respectively.

8- Future studies should further investigate the achievements of the present study by surveying and changing the tube back diameter by fixing the other side with the optimal arrangement, i.e., the cam-finned tube.

ACKNOWLEDGEMENTS

The authors thank the Faculty of Mechanical Engineering at Tikrit University and Northern Technical University, Technical Institute, Renewable Energy Research Unit, Hawija, Iraq. This work was supported by Tikrit University under Postgraduate Research Grant 3/7/16176 on 1/12/2021.

NOMENCLATURE

A_s	Surface area, m²
B	Bias error
c_p	Specific heat, kJ/(kg. K)
D_h	Hydraulic diameter, m
D_L	Longitudinal diameter, m
D_T	Transverse diameter, m
E	Input voltage, Volt
H	Domain height, m
h	Convection heat transfer coefficient, W/(m².K)
h_d	Height of downstream fins, m
h_u	Height of upstream fins, m
k	Thermal conductivity, W/(m.K)
L	Length, m
L_d	Downstream fin length, m
$\widehat{L_d}$	Dimensionless downstream fin length
L_u	Upstream fin length, m
$\widehat{L_u}$	Dimensionless upstream fin length
$\dot{m}$	Mass flow rate, kg/s
N	Number of samples
Nu	Nusselt number
n_d	Downstream fins number
n_u	Upstream fins number
P	Precision limit
p	Pressure, Pa
Pr	Prandtl number
q_{in}	Input heat transfer rate, W
Re	Reynolds number
S_L	Longitudinal Pitch, m
$\widehat{S_L}$	Dimensionless longitudinal pitch
S_T	Transverse Pitch, m

$\widehat{S_T}$	Dimensionless transverse pitches
T	Temperature, °C
u, v	Velocities in x- and y- directions, m/s
U, V	Dimensionless velocities in x- and y- directions
U_χ	uncertainty
W	Width, m
x, y	Cartesian coordinates
X, Y	Dimensionless cartesian coordinates
Greek Symbols	
α	Thermal diffusivity, m^2/s
θ	fins Angle °, Dimensionless temperature
$\hat{\theta}$	Dimensionless fin angle
v	Kinematic viscosity, m^2/s
μ	Dynamic Viscosity, kg/ms
ρ	Density, kg/m^3
σ	Standard deviations
χ	Scale
$\bar{\chi}$	Average value of the scale
π	Constant ratio
∞	ambient
Subscripts	
a	air
b	bulk
in	inlet
out	Outlet
s	surface
Abbreviation	
LFFTBHE	Longitudinally finned flat tubes bank heat exchanger
RSS	Root-Sum-Square

REFERENCES

[1] Dheyab HS, Al-Jethelah M, Ibrahim TK, Chtourou S, Baccar M. **Closed Solar Air Heater System Integrated with PCM (RT42 and RT50) in a Thermal Storage-Finned Heat Exchanger Unit.** *Tikrit Journal of Engineering Sciences* 2023; **30**(3):27-37.

[2] Hameed M, Mohammed HN, Abdullah MR. **The Improving the Thermal Performance of a Heat Exchanger Using a New Passive Technology.** *Tikrit Journal of Engineering Sciences* 2023; **30**(1):66-71.

[3] Buyruk E, Johnson MW, Owen I. **Numerical and Experimental Study of Flow and Heat Transfer around a Tube in Cross-Flow at Low Reynolds Number.** *International Journal of Heat and Fluid Flow* 1998; **19**(3):223-232.

[4] Dieck RH. **Measurement Uncertainty Models.** *ISA Transactions* 1997; **36**(1):29-35.

[5] Hausen H. **Heat Transfer in Counterflow, Parallel-Flow, and Cross-Flow.** 1983.

[6] Holman JP. **Experimental Methods for Engineers.** New York: McGraw-Hill 1966.

[7] Incropera FP, DeWitt DP, Bergman TL, Lavine AS. **Fundamentals of Heat and Mass Transfer.** Vol. 6. New York: Wiley; 1996.

[8] Khan MG, Fartaj A, Ting DSK. **An Experimental Characterization of Cross-Flow Cooling of Air via an In-Line Elliptical Tube Array.** *International Journal of Heat and Fluid Flow* 2004; **25**(4):636-648.

[9] Elghool A, et al. **Enhancing the Performance of a Thermo-Electric Generator through Multi-Objective Optimisation of Heat Pipes-Heat Sink under Natural Convection.** *Energy Conversion and Management* 2020; **209**:112626.

[10] Ibrahim TK, Basrawi F, Mohammed MN, Ibrahim H. **Effect of Perforation Area on Temperature Distribution of the Rectangular Fins under Natural Convection.** *ARPN Journal of Engineering and Applied Sciences* 2016; **11**(10):6371-6375.

[11] Liang C, Papadakis G. **Large Eddy Simulation of Cross-Flow through a Staggered Tube Bundle at Subcritical Reynolds Number.** *Journal of Fluids and Structures* 2007; **23**(8):1215-1230.

[12] Ahmed AH, Zaidan MH, Al-Jethelah MSM. **A Heat Transfer and Fluid Flow Characteristics in a TBHE Based on Constructal Design: An Overview.** *NTU Journal of Renewable Energy* 2023; **4**(1):57-96.

[13] Al-Jewaree HM. **An Experimentally Investigate the Fin Thermal Performance to the Different Fin Spaces by Natural Convections.** *Al-Kitab Journal for Pure Sciences* 2018; **2**(1).

[14] Mandhani VK, Chhabra RP, Eswaran V. **Forced Convection Heat Transfer in Tube Banks in Cross Flow.** *Chemical Engineering Science* 2002; **57**(3):379-391.

[15] Bahaidarah HMS, Ijaz M, Anand NK. **Numerical Study of Fluid Flow and Heat Transfer over a Series of In-Line Noncircular Tubes Confined in a Parallel-Plate Channel.** *Numerical Heat Transfer, Part B: Fundamentals* 2006; **50**(2):97-119.

[16] Ibrahim TK, et al. **Experimental and Numerical Investigation of Heat Transfer Augmentation in Heat Sinks Using Perforation Technique.** *Applied Thermal Engineering* 2019; **160**:113974.

[17] Ibrahim TK, et al. **The Impact of Square Shape Perforations on the Enhanced Heat Transfer from Fins: Experimental and Numerical Study.** *International Journal of Thermal Sciences* 2020; **149**:106144.

[18] Tahseen TA, Ishak M, Rahman MM. **Analysis of Laminar Forced Convection of Air for Crossflow over Two Staggered Flat Tubes.**

International Journal of Automotive and Mechanical Engineering 2012; **6**:755-767.

[19] Tahseen TA, Rahman MM, Ishak M. **An Experimental Study of Air Flow and Heat Transfer over In-Line Flat Tube Bank.** *International Journal of Automotive and Mechanical Engineering* 2014; **9**:1487-1500.

[20] Tahseen TA, Ishak M, Rahman MM. **An Experimental Study of Heat Transfer and Friction Factor Characteristics of Finned Flat Tube Banks with In-Line Tubes Configurations.** *Applied Mechanics and Materials* 2014; **564**:197-203.

[21] Tahseen TA, Ishak M, Rahman MM. **An Overview on Thermal and Fluid Flow Characteristics in a Plain Plate Finned and Un-Finned Tube Banks Heat Exchanger.** *Renewable and Sustainable Energy Reviews* 2015; **43**:363-380.

[22] Jassim AH, Tahseen TA, Mustafa AW, Rahman MM, Ishak M. **An Experimental Investigation in Forced Convective Heat Transfer and Friction Factor of Air Flow over Aligned Round and Flattened Tube Banks.** *Heat Transfer—Asian Research* 2019; **48**(6):2350-2369.

[23] Al Kumait AAR, Ibrahim TK, Abdullah MA. **Experimental and Numerical Study of Forced Convection Heat Transfer in Different Internally Ribbed Tubes Configuration Using TiO2 Nanofluid.** *Heat Transfer—Asian Research* 2019; **48**(5):1778-1804.

[24] Ibrahim TK, et al. **Experimental Study on the Effect of Perforations Shapes on Vertical Heated Fins Performance under Forced Convection Heat Transfer.** *International Journal of Heat and Mass Transfer* 2018; **118**:832-846.

[25] Tahseen TA, Ishak M, Rahman MM. **A Numerical Study of Forced Convection Heat Transfer over a Series of Flat Tubes between Parallel Plates.** *Journal of Mechanical Engineering and Sciences* 2012; **3**:271-280.

[26] Nada SA, El-Batsh H, Moawed M. **Heat Transfer and Fluid Flow around Semi-Circular Tube in Cross Flow at Different Orientations.** *Heat and Mass Transfer* 2007; **43**(11):1157-1169.

[27] Ibrahim TA, Gomaa A. **Thermal Performance Criteria of Elliptic Tube Bundle in Crossflow.** *International Journal of Thermal Sciences* 2009; **48**(11):2148-2158.

[28] Toolthaisong S, Kasayapanand N. **Effect of Attack Angles on Air Side Thermal and Pressure Drop of the Cross Flow Heat Exchangers with Staggered Tube Arrangement.** *Energy Procedia* 2013; **34**:417-429.

[29] Du X, Zeng M, Wang Q, Dong Z. **Experimental Investigation of Heat Transfer and Resistance Characteristics of a Finned Oval-Tube Heat Exchanger with Different Air Inlet Angles.** *Heat Transfer Engineering* 2014; **35**(6-8):703-710.

[30] Waheed A, Adil A, Razzaq A. **The Optimal Spacing between Diamond-Shaped Tubes Cooled by Free Convection Using Constructal Theory.** *Education* 2022; **2023**.

[31] Mustafa AW, Hussein Abdul Elqadir H. **Constructal Design of Multiscale Elliptic Tubes in Crossflow.** *Heat Transfer* 2020; **49**(4):2059-2079.

[32] Mustafa AW, Zahi JA. **The Optimal Spacing between Elliptic Tubes Cooled by Free Convection Using Constructal Theory.** *Al-Nahrain Journal for Engineering Sciences* 2017; **20**(3):762-769.

[33] Yehia Abbas N, Mustafa AW, Kheir Aldeen Abbas Asker M. **Constructal Design of Longitudinally Finned Tubes Cooled by Forced Convection.** *Heat Transfer* 2020; **49**(3):1613-1631.

[34] Rizal M, Ghani JA. **Design and Construction of a Strain Gauge-Based Dynamometer for a 3-Axis Cutting Force Measurement in Turning Process.** *Journal of Mechanical Engineering and Sciences* 2018; **12**(4):4072-4087.

[35] Ishak M, Tahseen TA, Rahman MM. **Experimental Investigation on Heat Transfer and Pressure Drop Characteristics of Air Flow over a Staggered Flat Tube Bank in Crossflow.** *International Journal of Automotive and Mechanical Engineering* 2013; **7**:900-911.

[36] Tahseen TA, Rahman MM, Ishak M. **Experimental Study on Heat Transfer and Friction Factor in Laminar Forced Convection over Flat Tube in Channel Flow.** *Procedia Engineering* 2015; **105**:46-55.

[37] Faghri M, Rao N. **Numerical Computation of Flow and Heat Transfer in Finned and Unfinned Tube Banks.** *International Journal of Heat and Mass Transfer* 1987; **30**(2):363-372.

[38] Naik S, Probert SD, Shilston MJ. **Forced-Convective Steady-State Heat Transfers from Shrouded Vertical Fin Arrays, Aligned Parallel to an**

Undisturbed Air-Stream. *Applied Energy* 1987; **26**(2):137-158.

[39] Tahseen TA. **Optimal Geometric Arrangement of Unfinned and Finned Flat Tube Heat Exchangers under Laminar Forced Convection.** Ph.D Thesis, Universiti Malaysia Pahang; 2014.

[40] Tahseen TA, Ishak M, Rahman MM. **Performance Predictions of Laminar Heat Transfer and Pressure Drop in an In-Line Flat Tube Bundle Using an Adaptive Neuro-Fuzzy Inference System (ANFIS) Model.** *International Communications in Heat and Mass Transfer* 2014; **50**:85-97.

[41] Bello-Ochende T, Bejan A. **Maximal Heat Transfer Density: Plates with Multiple Lengths in Forced Convection.** *International Journal of Thermal Sciences* 2004; **43**(12):1181-1186.

[42] Rogers GFC, Mayhew YR. **Thermodynamic and Transport Properties of Fluids.** John Wiley & Sons; 1995.

[43] Matos RS, Vargas JVC, Laursen TA, Bejan A. **Optimally Staggered Finned Circular and Elliptic Tubes in Forced Convection.** *International Journal of Heat and Mass Transfer* 2004; **47**(6-7):1347-1359.

[44] Stanescu G, Fowler AJ, Bejan A. **The Optimal Spacing of Cylinders in Free-Stream Cross-Flow Forced Convection.** *International Journal of Heat and Mass Transfer* 1996; **39**(2):311-317.

[45] Muste M, et al. **Experimental Hydraulics: Methods, Instrumentation, Data Processing and Management: Volume I: Fundamentals and Methods.** CRC Press; 2017.

[46] Figliola RS, Beasley DE. **Theory and Design for Mechanical Measurements.** John Wiley & Sons; 2014.

[47] Kim YY, Kim KS, Jeong GH, Jeong S. **An Experimental Study on the Quantitative Interpretation of Local Convective Heat Transfer for a Plate Fin and Tube Heat Exchanger Using the Lumped Capacitance Method.** *International Journal of Heat and Mass Transfer* 2006; **49**(1-2):230-239.

[48] Moffat RJ. **Using Uncertainty Analysis in the Planning of an Experiment.** 1985.

[49] Hashim Hussein Y, Akroot A, Tahseen TA. **Investigation of Free Convection Heat Transfer from Vertical Cylinders with Semicircular Fins.** *Experimental Heat Transfer* 2023:1-20.

[50] Razera AL, et al. **Fluid Flow and Heat Transfer Maximization of Elliptic Cross-Section Tubes Exposed to Forced Convection: A Numerical Approach Motivated by Bejan's Theory.** *International Communications in Heat and Mass Transfer* 2019; **109**:104366.

[51] Ibrahim E, Moawed M. **Forced Convection and Entropy Generation from Elliptic Tubes with Longitudinal Fins.** *Energy Conversion and Management* 2009; **50**(8):1946-1954.

[52] Cengel YA, Ghajar AJ. **Heat and Mass Transfer.** McGraw-Hill Education; 2015.

[53] Yadav R. **Applied Thermodynamics.** IK International Pvt Ltd; 2024.

[54] Abraham B, Ledolter J. **Student Solutions Manual for Introduction to Regression Modeling.** Thomson Brooks/Cole; 2006.

[55] Lin J-G, Wei B-C. **Testing for Heteroscedasticity and/or Correlation in Nonlinear Models with Correlated Errors.** *Communications in Statistics-Theory and Methods* 2004; **33**(2):251-275.

[56] Junqi D, Jiangping C, Zhijiu C, Yimin Z, Wenfeng Z. **Heat Transfer and Pressure Drop Correlations for the Wavy Fin and Flat Tube Heat Exchangers.** *Applied Thermal Engineering* 2007; **27**(11-12):2066-2073.